Functional Materials 17, No.1 (2010)

Properties of amorphous and crystalline surfaces of nano-hydroxyapatites

Yu.Sakhno, L.Bertinetti, G.Martra, S.Coluccia, A.Tampieri[*]*, N.Roveri*[**]

Dip. di Chimica IFM and NIS Center of Excellence, Universita di Torino, Via P.Giuria 7, 10125 Torino, Italy
[*]ISTEC-CNR, Via Granarolo 64, 48018 Faenza, Italy
[**]Dip. di Chimica "G.Ciamician" Universita di Bologna, Via F.Selmi 2, 40126 Bologna, Italy

Received September 2, 2009

Two nano-hydroxyapatite materials being similar in morphology but different in surface structure (crystalline and including a 1 to 2 nm thick amprphous layer) have been studied by high resolution transmission electron microscopy and FTIR spectroscopy in vacuum and using *in situ* CO and H_2O. These materials have been shown to have similar stoichiometry and carbonate content. The properties of surface cationic sites and the structure of water adlayers are considered in detail.

Методом просвечивающей электронной микроскопии высокого разрешения и Фурье ИК-спектроскопии в вакууме и с применением *in situ* CO и H_2O исследованы два нано-гидроксиапатитных материала, аналогичных по морфологии, но различных по структуре поверхности: кристаллической и с наличием аморфного слоя толщиной 1-2 нм. Показано, что эти материалы имеют аналогичную стехиометрию и содержание карбоната. Рассмотрены свойства поверхностных катионных узлов и структура слоев адсорбированной воды.

1. Introduction

Hydroxyapatite (HAp) $Ca_{10}(PO_4)_6(OH)_2$, is the main inorganic component of hard tissues in bone and teeth, which is widely used in various biomedical applications due to its excellent biocompatibility and bioactivity [1–3]. Now the interest in this material grows due to HAp implications in many fields including nanotechnology [4], biomaterials [5], biomineralization [6, 7], biotechnology [8–10], drug delivery systems [11, 12], bone tissue engineering [13, 14], bioseparations [15], etc.

The processes of both HAp crystal growth on a surface and controllable synthesis of these crystals are well studied and described in literature (see. [16, 17], respectively). According to investigation [18], the surface of micrometer size HAp particles is limited by well-defined crystal planes fixed by the $P6_3/m$ space group of the calcium hydroxyapatite. These planes contain two types of binding sites, so-called C and P ones: the former are arranged in a rectangular arrays on *ac* or *bc* faces rich in calcium ions which act as adsorbing sites for acidic proteins; the latter sites are arranged hexagonally on the *ab* faces only and depleted of calcium ions being adsorbing sites for basic proteins. Nowadays, it is of very interest to verify such behavior for nanostructured HAp that were found to be able of better performances *in vitro* test with osteoblast [19]. Moreover, recent investigations of nano-HAp reveal occurrence of amorphous, non-apatitic surface layer surrounding the crystalline HAp bulk [20].

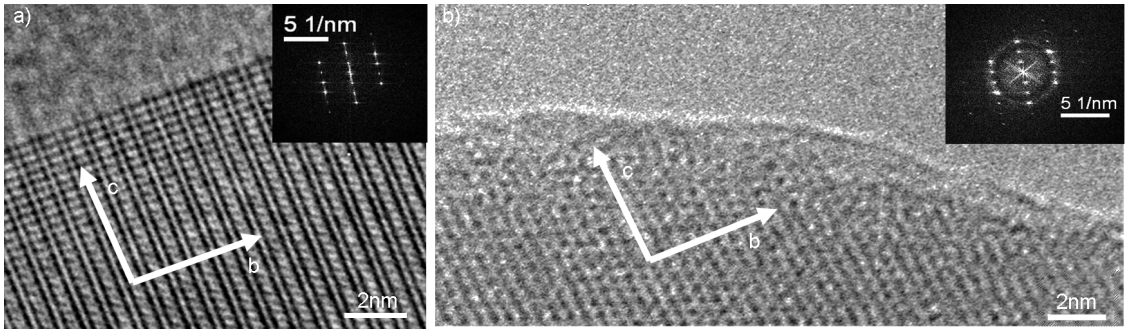

Fig. 1. HRTEM micrographs: a) HApC particle along *c* axis; b) HApA particle with the amorphous surface layer. Insets: Fourier Transforms of related images.

In this paper, we present the comparative study results of the HAp nanoclusters that appear to be limited by amorphous layer or crystalline surfaces, depending on the preparation method. Our work is based on making use of combined multi-technique study, being Ultra High Resolution Transmission Electronic Microscopy (UHR-TEM) and Fourier Transformation Infrared (FTIR) spectroscopy.

2. Experimental

Two similar hydroxyapatite powders, being HApA (hydroxyapatite with amorphous surface) and HApC (hydroxyapatite with crystalline surface), were used to investigate their surfaces. The synthesis methods have been described in our previous works [17, 20]. For IR measurements, highly pure CO (Praxair) was employed without any additional purification, except for liquid nitrogen trapping, which was used for CO admission (99.9 at. % D, Aldrich).

For the powder investigation by UHR-TEM, a JEOL EX4000 with 400 kV acceleration potential and a JEOL 3010-UHR with 300 kV acceleration potential were used. The samples were dispersed on lace carbon Cu gauzes. The image calculations for the analysis of the experimental data taken with the JEOL EX4000 instrument were made basing on the online version of EMS software package [21] using the Bloch wave method for different values of crystal thickness and objective defocusing. The FTIR spectra were obtained using a Bruker Vector 22 spectrometer with 4 cm^{-1} resolution equipped with DTGS or MCT detector for ATR and transmission mode, respectively. Infrared spectra for the analysis of surface features were taken in transmission mode on HAp powders pressed in self-supporting pellets. The samples were placed in a quartz IR cell equipped with KBr windows designed to carry out spectroscopic measurements both at beam temperature (ca. 50°C) and low temperature (ca. −170°C, under liquid nitrogen cooling). The cell was connected to a conventional vacuum line with residual pressure 10^{-5} mbar = 10^{-3} Pa that allows one to carry out all thermal treatments and adsorption-desorption experiments *in situ*. The spectra of adsorbed CO are recorded in absorbance and corrected for the background. The specific surface area of the samples was determined using the conventional BET technique based on the low-temperature nitrogen adsorption [22].

3. Results and discussion

Both above samples exhibit elongated particles of 50–150 nm length and 10–70 nm width in projection on the image plane, where these particles are seen to have rounded edges and platelet morphology. In the HApC case, the particles are characterized by the platelet thickness being halved with respect to other two dimensions. As for HApA, the particles exhibit comparable values of both width and thickness to form stacked agglomerates with the particle orientations mainly along their lengths. Sometimes, they are actually joined through amorphous structure grain boundaries to form larger secondary nanostructured particles. Such morphological differences result in a small difference in specific surface area of the materials, being 70 m^2/g for HApC and 80 m^2/g for HApA.

Observations in high-resolution conditions allow us to provide insights into both bulk and surface structures of the materials investigated. As is seen in Fig. 1b, in the HApA case, the particles are elongated along the *c*-axis to be perfectly crystalline within their bulk, while near the surface, the crystal structure is transformed into 1–2 nm thick amorphous layers. In contrast, in the HApC particles, the crystalline order-

ing extends up to the surface (Fig. 1a). Of interest is that UHR-TEM indicates the extended surfaces of the platelets to be parallel to both *b* and *c* crystal axes, so that the material exposes mainly planes of the {100} family with a regular pattern of calcium and phosphate ions being typical for such surfaces [23].

The possible differences in the Lewis acid strength of cationic sites at the surfaces of the two materials have been assessed. This investigation has been performed by IR measurements of adsorbed CO as a vibrational probe highly sensitive to the features of Ca^{2+} exposed ions. In fact, if CO molecules are adsorbed on surface of Ca^{2+} sites due to electrostatic interaction [24], this results in an upward shift of the stretching frequency of adsorbed CO, which increases the Lewis acid strength of the adsorbing centers. To provide an access to surface sites, the materials have to be outgassed in vacuum at temperatures exceeding the room temperature, because the sample surfaces are naturally hydrated. However, as the HAp surface undergoes the stronger reconstructions, the higher outgassing temperature [20] is, we fix it so that the most of the water molecules is removed off a surface without significant modification of the structure, namely at 130°C for HApA and 160°C for HApC.

Fig. 2 shows the spectra within the $\nu_{(CO)}$ regions that were obtained for decreasing coverage of CO adsorbed on HApA and HApC, respectively. For both materials, the position of the $\nu_{(CO)}$ band and its evolution with coverage decrease is seen to be very similar: at high CO coverage, a rather intense band with maximum at 2168 cm^{-1} is observed to be slightly asymmetric on the low-frequency branch. With decreasing coverage, the band intensity decreases progressively so that its maximum is shifted towards higher frequency. In the last stages, the band profile appears quite broadened because of the contribution from the component at ca 2180 cm^{-1}. The active sites responsible for this component are slightly more resistant to the outgassing process, so that IR spectra are progressively broadened and moved toward high frequencies.

The above-mentioned similarity in the IR spectra indicates that, despite the relevant structural differences from the crystal, the amorphous surfaces of HApA expose Ca^{2+} ions. This conclusion is confirmed by matching of both surfaces HApA and HApC in terms of Lewis acidity.

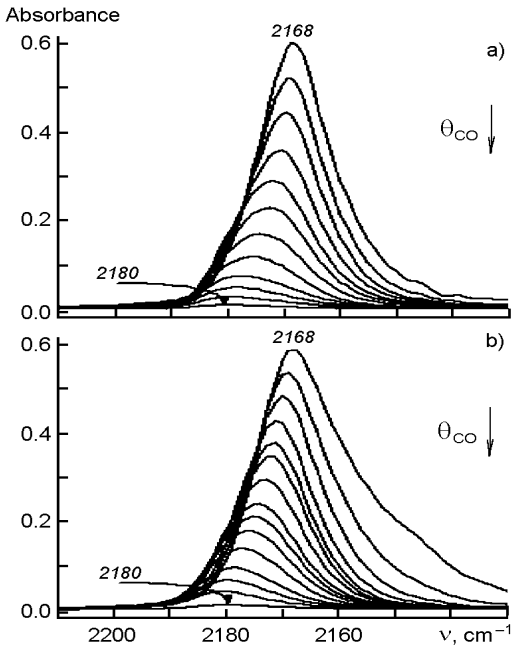

Fig. 2. IR spectra of CO adsorbed at ca 100 K on HApA outgassed at 130°C (a) and on HApB outgassed at 160°C (b)

From the studies [24] carried out on the basis of comparison of Lewis acidity of calcium phosphate and HAp, we can conclude that in the HApA case, there are two spectral components caused by the presence of two Ca^{2+} cation families on the surfaces with different Lewis acidity, though the stronger one constitutes a minor fraction.

To study the structure of water layers at the interface of the materials investigated, a small amount of H_2O (from 0.01 mbar of the water vapor pressure) was admitted to the samples pre-outgassed at the above temperatures. The evolution of the stretching modes of H_2O, whose spectra are the most sensitive to the structure of the H-bond network, was investigated by IR spectroscopy (see Fig. 3, a and b). To obtain the information related to the water interface only, the spectra of increasing coverage have been subtracted from the spectra of the materials outgassed (spectra a in Fig. 3 a and b). The resulting absorption spectra for HApA and HApC are shown in Fig. 3 c and d, respectively.

At low coverage, a very broad band extending over the 3700–2600 cm^{-1} range and centered at about 3300 cm^{-1} can be observed for both materials. As the coverage increases, the band appears to be structurized into two main components at about

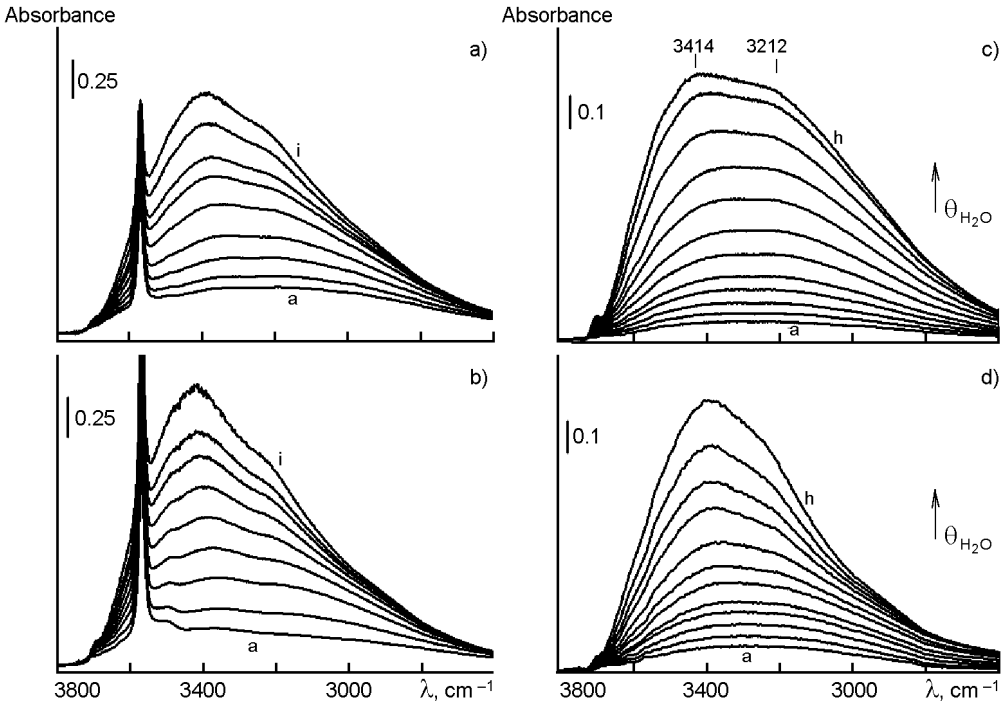

Fig. 3. IR spectra of the $\nu(H_2O)$ region of HApA (a) and HApC (b), being outgassed (curves a) and after increasing water vapour pressure (curves b–i). Spectra c and d are rebuilt after subtracting spectrum of outgassed material.

3400 cm^{-1} and 3200 cm^{-1}. At high coverage, the component at higher frequency grows more intensively than the other one. However, in the case of HApA, the lower-frequency component is only slightly more intense than the one for HApC being much weaker; the resulting $\delta(H_2O)$ band at high coverage is narrower in the case of the material with ordered surfaces.

Thus, the spectra of both samples related to low coverage are almost indistinguishable together with chemical activity of the surface sites being identical in both cases. Because the surface structure affects the structure of water adlayers, amorphous surfaces induce a water structure on interfaces characterized by a stronger H-network with respect to atomically ordered surfaces (that is confirmed by the broader stretching band at high coverage).

4. Conclusions

Comparing two kind of nano-hydroxyapatites with similar morphological and compositional features but with different surface structure (crystalline and amorphous), it has been found that Ca^{2+} cationic sites exposed at the surface of the two materials exhibit a similar Lewis acid strength. The same active sites are involved in water adsorption, but, provided by FTIR spectra of OH-region sensitive to the water structure, show that mainly the first layer of water indicates the same structure thereof. In contrast, starting from the second layer, the water structure rearrangement of the becomes more evident. The temperatures have been established at which most of the water is removed without significant modifications in surface structure, namely 130°C and 160°C for amorphous and crystalline hydroxyapatites, respectively. The structure of water adsorbed on crystalline hydroxyapatites resembles a liquid-like state, while conformation of water for amorphous hydroxyapatites sample are different. This allows us to conclude that different surfaces of hydroxyapatite affect the water conformation in adlayers, which play a relevant role in biocapability.

References

1. S.Mann, *Nature*, **332**, 119 (1988).
2. K.Furuichi, Y.Oaki, H.Imai, *Chem.Mater.*, **18**, 229 (2006).
3. Z.H.Zhou, P.L.Zhou, Sh.P.Yang et al., *Mater. Res.Bull.*, **42**, 1611 (2007).
4. J.J.Gray, *Curr.Opin.Struct.Biol.*, **14**, 110 (2004).
5. T.Vo-Dinh, Nanotechnology in Biology and Medicine: Methods, Devices, and Applications, Taylor & Francis Group, Boca Raton, FL (2007).

6. B.D.Ratner, A.S.Hoffman, F.J.Schoen, J.Lemons, Biomaterials Science: an Introduction to Materials in Medicine, 2nd edition, Academic Press, Elsevier, Amsterdam (2004).
7. L.L.Hench, J.M.Polak, *Science*, **295**, 1014 (2002).
8. V.Dubok, L.Ivanchenko et al., *MetalloFiz. Noveish. Tekhnol.*, **3**, 102 (1997).
9. T.Kokubo, H.Kushitani, S.J.Sakka, *Biomed. Mater. Res. Symp.*, **24**, 721 (1990).
10. J.Song, V.Malathong, C.R.Bertozzi, *J. Am. Chem. Soc.*, **127**, 3366 (2005).
11. B.Palazzo, M.C.Sidoti, N.Roveri, *R. Mater. Sci. Eng. C*, **25**, 207 (2005).
12. M.Vallet-Reg, *Chem. Eur. J.*, **12**, 5934 (2006).
13. N.Hijon, M.V.Cabanas, I.Izquierdo-Barba, M.Vallet-Reg, *Chem. Mater.*, **16**, 1451 (2004).
14. A.P.Tomsia, E.Saiz, J.Song, C.R.Bertozzi, *Adv. Eng. Mater.*, **7**, 999 (2005).
15. E.Schroder, T.Jonsson, L.Poole, *Anal. Biochem.*, **313**, 176 (2003).
16. A.S.Kryzhanovskaia, A.V.Tolmachev, In Relev. Problems of Modern Mater. Sci., Kiev, Akademperiodika, V. 2, p. 202 (2008) [in Russian].
17. P.Barbara, D.Walsh, M.Iafisco et al., *Acta Biomater.*, **5**, 1241(2009).
18. K.Kandori, A.Fudo, T.Ishikawa, *Colloids Surf. B*, **24**, 145 (2002).
19. T.J.Webster, R.W.Siegel, R.Bizios, *Biomaterials*, **21**, 1803 (2000).
20. L.Bertinetti, A.Tampieri, G.Martra et al., *J. Phys. Chem. C*, **111**, 4027 (2007).
21. P.A.Stadelmann, *Ultramicroscopy*, **21**, 131 (1987).
22. G.M.Bliznakov, I.V.Bakardjiev, E.M.Gocheva, *J. Catal.*, **18**, 260 (1970).
23. M.Corno, C.Busco, P.Ugliengo et al., *Langmuir*, **25**, 2188 (2009).
24. K.I Hadjiivanov, G.N.Vayssilov, *Adv. Catal.*, **47**, 307 (2002).

Властивості аморфної та кристалічної поверхні нано-гідроксіапатитів

Ю.Сахно, Л.Бертінетті, Дж.Мартра, С.Колучча, А.Тампієрі, Н.Ровері

Методом просвічувальної електронної мікроскопії високого розрішення та Фур'є ІЧ-спектроскопії у вакуумі та з застосуванням *in situ* CO та H_2O досліджено два нано-гідроксіапатитних матеріали, аналогічні по морфології, але відмінних по структурі поверхні: кристалічної та з наявністю аморфного шару товщиною 1-2 нм. Показано, що ці матеріали мають аналогічну стехіометрію та вміст карбонату. Розглянуто властивості поверхневих катіонних вузлів та структуру шарів адсорбованої води.